Journal of Composite Materials

http://jcm.sagepub.com/

# Multi-scale Analyses of 3D Woven Composite Based On Periodicity Boundary Conditions

X.F. Wang, X.W. Wang, G.M. Zhou and C.W. Zhou

*Journal of Composite Materials* 2007 41: 1773
DOI: 10.1177/0021998306069891

The online version of this article can be found at:
http://jcm.sagepub.com/content/41/14/1773

Published by:
SAGE
http://www.sagepublications.com

On behalf of:
American Society for Composites

# Multi-scale Analyses of 3D Woven Composite Based On Periodicity Boundary Conditions

X. F. WANG,* X. W. WANG, G. M. ZHOU AND C. W. ZHOU
*College of Aerospace Engineering, Nanjing University of Aeronautics and Astronautics, Nanjing 210016, P.R. China*

**ABSTRACT:** In this article, two-scale 3D finite element (FE) models, the microscopic repeated unit cell (RUC) model for yarn, and mesoscopic-repeated unit cell model for woven composite, are presented to predict the effective stiffness properties of 3D woven orthogonal interlock composites. The micro-RUC model for the yarn is based on a hexagonal array of fibers. Undulation of the yarns in the novel 3-D meso-RUC for the woven composite is described by Hermit-spline function. The periodic boundary conditions are applied to the two-scale models during the 3D FE analysis in order to ensure that both the displacement and stress are continuous on the boundary surfaces. Specimens are manufactured with house-made resin transfer molding (RTM) equipment and simple tensile experiment is performed. It is found that the predicted yarn properties by the micro-RUC agree well with data computed by equations with a suitable parameter determined by experiment and the predicted effective stiffness properties of 3-D woven composites by the meso-RUC are also in good agreement with the test data. Thus the correctness of the established multi-scale models and analysis method are verified.

**KEY WORDS:** 3D woven composite, multiple scale analyses, periodic boundary conditions, experiment.

## INTRODUCTION

THE 3D WOVEN composite is a spatial net-shape fabric, formed by interlacing binding threads in the thickness direction to join layers of warp and weft together, and cured with matrix under certain condition. The material is more advantageous than the plane woven laminated composite for its high damage tolerance, high impact resistance, and low fabrication cost. Consequently, 3D woven composite material has been widely used in aerospace, automobile, marine, and defense industries.

*Author to whom correspondence should be addressed. E-mail: xinfengw@nuaa.edu.cn
Figures 3, 4 and 6 appear in color online: http://jcm.sagepub.com



0021-9983/07/14 1773–16 $10.00/0 DOI: 10.1177/0021998306069891

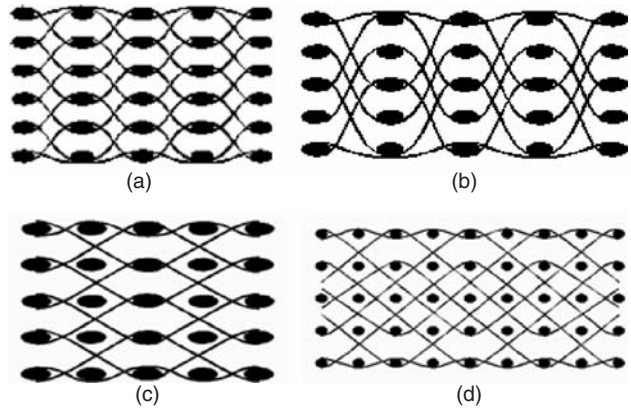


***Figure 1.*** *3D woven constitutions: (a), (b) orthogonal interlock; (c), (d) angle interlock.*

The often-used 3D woven composites include those of orthogonal interlock and angle interlock typically as shown in Figure 1, although there are many forms with the variations of interlock depth in thickness direction of warp yarn.

For effective use and design of 3D woven composites, one should understand their mechanical behavior clearly. Several models [1,2] have recently been suggested to predict their mechanical properties. The micro-mechanical model and analysis method for 3D woven composites are, however, distinctly different from those for plane woven laminates. The studies have been focused on the following two aspects: one is the description of the micro geometric structure of the model and the other is the analysis method adopted.

As to the micro geometric structure, attention is focused on the shape of cross-section of the yarns and undulating tracks of longitudinal yarns. Based on the conjecture that warp and weft were tightly contacted, the micro geometry structures were obtained [3–6] by assuming the shapes to be reticular, elliptic, racetrack, or sinusoidal. Yang [7] used cubic polynomial to simulate the track of warp and weft, and predicted the stiffness for the cross-bend plate.

As to the analysis methods, two categories can be classified, analytical methods and numerical ones. Most analytical models are based on the classical laminate theory (CLT). Elastic properties were obtained by averaging the stiffness constants integrated along crimple yarns [3–5,7–9]. Yi and Ding [10] proposed a four sub-unit cell model for textile composites, namely warp, filling, stuffer, and binder, and simulated the stress–strain relationship by a method termed as the effective response comparison technique. Zhou et al. [6] suggested a unit cell composed of two phases of 3D woven composites and obtained the elastic properties by using the Galerkin method. The above-mentioned analytical methods cannot provide details of the microstructure and micro stresses of the composites such as the interactions between conjunct yarns. Accurate prediction of micro-stress distribution may have significant effect on the strength predictions since damage largely depends on local stress characteristics in each phase of composites. There were several numerical models proposed recently for analysis of 3D braided composites, such as the binary model by Coxet et al. [11], in which fiber yarns were simulated by bar elements and effective matrix by brick elements, and 3D FE models [12,13], where brick elements were used. However, the application of numerical method to 3D woven composites is relatively few. This might partly be attributed to the complexity

in construct an appropriate RUC model and in application of correct periodic boundary conditions.

Although a number of models are available for predicting mechanical properties of 3D woven composites, each model has its limitations. For example, all CLT-based models under-predict the shear modulus because of the rule of mixtures assumption intrinsic to CLT. Furthermore, textile composites have a feature of an inherent structural hierarchy in a variety of length scales, i.e. (a) the fiber diameter scale, (b) the yarn-diameter scale, (c) the meso-repeated unit cell scale, and (d) the macro-structural component scale. It is desirable to start from the micro-geometry and to obtain the behavior of the composite structure step by step by performing the multi-scale analysis [14]. Although the microscopic behaviors of fiber yarns can be predicted by equations with suitable parameters, the parameters need to be determined by experiments. The aim of this work is to develop more accurate two-scale 3D finite element models for 3D woven orthogonal interlock composites. Based on the properties of two basic constituents of the composite, fiber and matrix, the yarn properties are first obtained through FE analysis on the micro-RUC model. Next, the mechanical properties of the composite are obtained through analysis of a meso-RUC model, representing the geometry of the warp and weft yarns with higher fidelity to the actual composite. A key to success of the multi-scale analysis is the application of accurate periodic boundary conditions to the micro- and meso-scale RUCs, which ensure that both the displacement and tractions are continuous on the boundary surfaces. The predicted results by the current method are compared with either analytical or experimental data of the yarns and the 3D woven composites and they are in good agreement.

## PERIODIC BOUNDARY CONDITIONS

Xia et al. [15,16] have developed an explicit unified form of periodic boundary conditions and used it in FEM analyses of RUCs for unidirectional and angle-ply laminates. Since the 3D woven composite materials can also be envisaged as a periodical array of RUCs, the periodic boundary conditions will be adopted in this analysis. For the sake of completeness it is shortly summarized in the following.

The displacement field for a periodic structure can be expressed as:

$$u_i(x_1, x_2, x_3) = \bar{\varepsilon}_{ik} x_k + u_i^*(x_1, x_2, x_3) \tag{1}$$

where $x_k$ is the Cartesian coordinate of a material point and $\bar{\varepsilon}_{ik}$ are the average strains over the RUC. The first term on the right-hand side represents a linear distributed displacement field, and the second term on the right-hand side, $u_i^*(x_1, x_2, x_3)$, is a periodic function from one RUC to another.

Since the periodic array of RUCs represents a continuous physical body, two continuity conditions must be satisfied at the boundaries of neighboring RUCs. One condition is that the displacements must be continuous; it implies that each RUC in the composite has the same deformation mode and that there is no separation or overlap between neighboring RUCs. The other condition implies that the traction distributions at the opposite parallel boundaries of a RUC must be the same. In this manner, individual RUCs can be assembled as a physically continuous body.

Equation (1) meets the first requirement. However, it cannot be directly applied to the boundaries because the periodic part, $u_i^*(x_1, x_2, x_3)$, is generally unknown.

It is noticed that for most RUCs the boundary surfaces always appear in parallel pairs. Displacements on a pair of parallel opposite boundary surfaces (with their normal along the $X_j$ axis) can be written as:

$$u_i^{j+} = \bar{\varepsilon}_{ik} x_k^{j+} + u_i^* \tag{2}$$

$$u_i^{j-} = \bar{\varepsilon}_{ik} x_k^{j-} + u_i^* \tag{3}$$

where index '$j+$' means along the positive $X_j$ direction and '$j-$' means along the negative $X_j$ direction, respectively.

Since $u_i^*(x_1, x_2, x_3)$ is the same at the two parallel boundaries, the difference between the above two equations is:

$$u_i^{j+} - u_i^{j-} = \bar{\varepsilon}_{ik}(x_k^{j+} - x_k^{j-}) = \bar{\varepsilon}_{ik} \Delta x_k^j. \tag{4}$$

The right hand side of Equation (4) becomes constant with specified $\bar{\varepsilon}_{ik}$, since $\Delta x_k^j$ are constants for each pair of the parallel boundary surfaces. Equation (4) can be readily applied as the nodal displacement constraint equation in finite element analysis.

It is assumed that the average mechanical properties of a RUC are equal to the average properties of a particular composite. The average stresses in a RUC are defined by:

$$\bar{\sigma}_{ij} = \frac{1}{V} \int_V \sigma_{ij} \, \mathrm{d}V \tag{5}$$

where $V$ is the volume of the repeated unit cell.

The 3D woven orthogonal interlock composite is assumed to be orthotropic and linearly elastic. In a matrix notation form, the constitutive relation of this material can be written as:

$$\{\bar{\varepsilon}\} = [S]\{\bar{\sigma}\} \tag{6}$$

where [S] is the compliance matrix. Once $\bar{\sigma}_{ij}$ of a RUC are obtained for given $\bar{\varepsilon}_{ij}$ by Equation (5), the $S_{ij}$ can be determined by Equation (6). Then, the engineering elastic constants of the material can be computed from the $S_{ij}$.

## MULTI-SCALE RUC MODELS

As explained in the Introduction, two types of RUC models have been developed.

### Micro-RUC Model of Yarns

Yarns are considered as unidirectional fiber reinforced composite which is idealized as periodic array of fibers in the matrix with fiber volume fraction equal to the

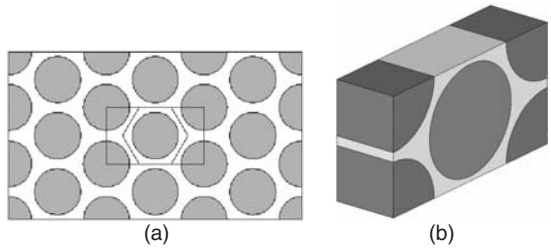


***Figure 2.*** *Fiber distribution pattern: (a) fiber distribution and (b) micro-mechanical model of yarns.*

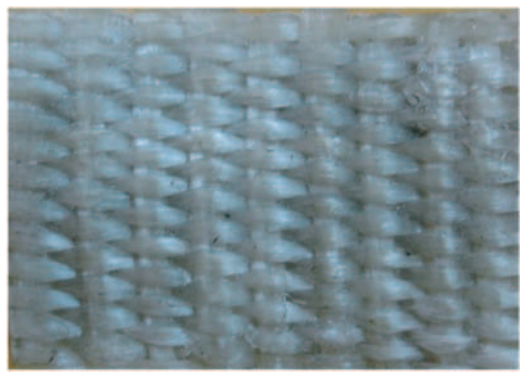

***Figure 3.*** *Photo of fabric.*

packing density. A great deal of mechanical models, such as rectangular cross-section model [16,17], column model [18], and hexagonal model [19], has been studied. Among them, the hexagonal model is widely quoted for modeling transversely isotropic material. Since the periodical boundary conditions, Equation (4), cannot be used easily in the hexagonal model, a rectangular micro-RUC model containing the hexagonal model is adopted herein as shown in Figure 2. Thus, the periodical boundary conditions can be easily applied during finite element analysis.

## Meso-RUC of 3D Woven Composite

The 3D woven orthogonal interlock composite is considered in this paper. The warp interlocks with two layers of weft in thickness direction (Figure 3). The warp and the weft are both 480Tex S-glass fiber with the linear densities of 480 g/km. The density of yarns in the fabric is characterized by the number of ends and picks per centimeter $P_{\mathrm{Wa}}$ and $P_{\mathrm{We}}$ with values of 10 and 3.5, respectively. The thickness of the composite is 4 mm consisting of seven layers of warp and six layers of weft. The micro-picture of a typical cross-section of the 3D woven composite in the warp and weft direction (Figure 4) shows that weft yarns are slightly wavy and the warp yarns bent at the interact area, but all other parts are straight lines because of the pull force of the textile machine.

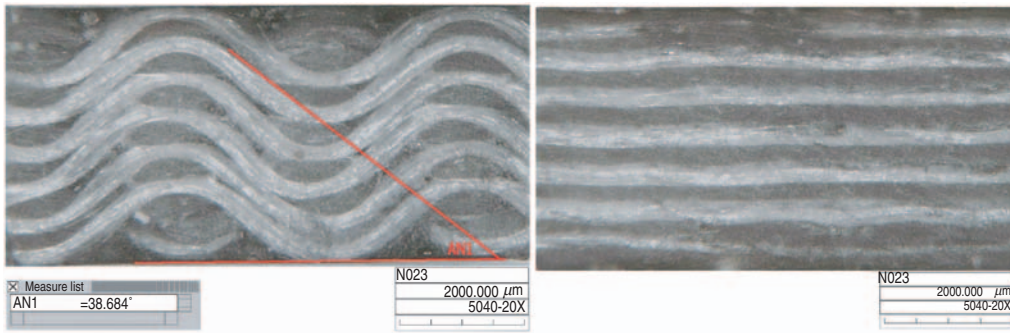


***Figure 4.*** *Photos of the composite: (a) warp direction and (b) weft direction.*

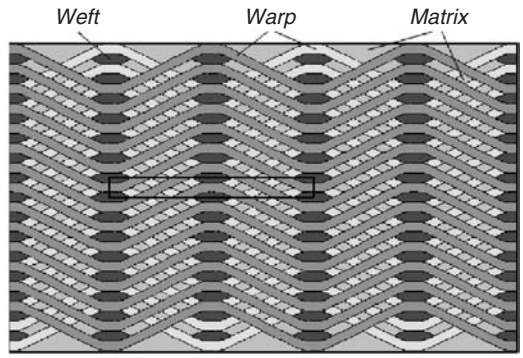


***Figure 5.*** *The idealized micro-architecture.*

Three assumptions are made in construction of geometry of the meso-RUC model:

- The weft yarns are considered as straight bundles of fibers.
- The warp and weft yarns have the same shape and area of cross-section and the shape of cross-section of yarns stay unchanged along their tracks.

The idealized micro architecture of the 3D woven composite material is shown in Figure 5.

Figure 3 shows that warp yarns contact closely to each other due to the high warp density. Therefore, it is assumed that the width of the cross-section of yarns, $a$, equals $1/P_{\mathrm{Wa}}$, and the height of the cross-section of yarns, $b$, can be determined by the thickness of the composite and the total numbers of layers of warp and weft yarns. Even if the width and height of the cross-section of yarns are known, however, the shape of the cross-section of yarns still cannot be exactly described. In order to describe the shape, the Hermit-spline curve is adopted herein, since the 3D crimp model has been widely used in analyses of plain-woven composites.

The typical binding form of warp and weft yarns is shown in Figure 6. It is assumed that the warp yarns and the weft yarns are contacted closely. Then the inclined angle $\theta$ of the straight part of warp yarns can be determined geometrically. The shape of the cross-section of yarns is supposed to be symmetric with two parts, a rectangle and two

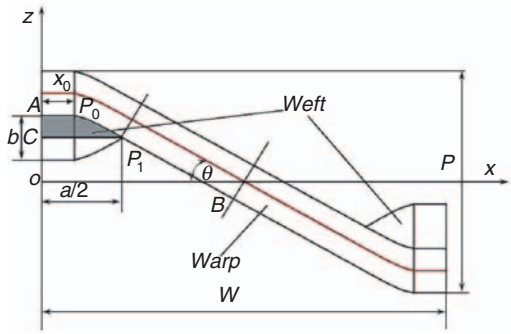


***Figure 6.*** *Typical binding form of warp and weft yarns.*

curved triangles. The curved side of the shape, e.g., $P_0P_1$ in Figure 6, can be described by a Hermit-spline curve expressed by:

$$P(t) = P_0 \cdot F_0(t) + P_1 \cdot F_1(t) + P_0^{'} \cdot G_0(t) + P_1^{'} \cdot G_1(t) \quad (t \in [0,1]) \tag{7}$$

where $P_0$ and $P_1$ are the two end points, namely points of $(x_0, 3b/2)$ and $(a/2, b)$; $P_0^{'}$ and $P_1^{'}$ are the tangential vectors at the two ends with values of (1, 0) and $(\cos\theta, -\sin\theta)$; $t$ is a parameter varying from 0 to 1. Base functions of Hermit-spline are:

$$\left.\begin{aligned} F_0(t) &= 2t^3 - 3t^2 + 1 \\ F_1(t) &= -2t^3 + 3t^2 \\ G_0(t) &= t(t-1)^2 \\ G_1(t) &= t^2(t-1) \end{aligned}\right\}. \tag{8}$$

Given coordinates of two end points, a fairly smooth curve can be produced due to the geometric invariant of triplicate Hermit-spline function. The remaining undetermined variable is $x_0$, abscissa of $P_0$ varying between 0 to $a/2$. In the present model, the shape is adjusted by changing $x_0$ to make the area enclosed by $A$–$P_0$–$P_1$–$C$, the shaded area shown in Figure 6, a quarter of actual cross-section area of impregnated yarns. In this way, the shape of the cross-section of yarns is uniquely determined and the trace of warp is also obtained.

An assumption is made that there is enough number of layers so the effect of surface yarns on the prediction is negligible. A rectangle block shown in Figure 5 can be selected to be the meso-RUC for the 3-D woven composite. Figure 7 shows the details of warp fibers and weft fibers in the RUC. Note that the neighboring warps have a shift of a half width of the RUC (W as shown in Figure 6), the length of the RUC in the $y$-direction must be equal to twice the width of the cross-section area of the yarn.

## RESULTS AND DISCUSSIONS

### Predicted Material Constants for Yarn

The fiber volume fraction of the impregnated yarns is 87% and material constants of resin and fibers are listed in Table 1. A finite element model of micro-RUC for yarn

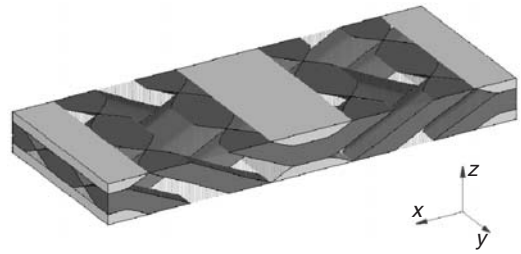


***Figure 7.*** *RUC of the 3D woven composite.*

***Table 1. Elastic property of resin and fiber.***

| Materials | E (GPa) | $\upsilon$ |
|---|---|---|
| S-glass fiber | 86.0 | 0.20 |
| Epoxy matrix | 3.5 | 0.35 |

is shown in Figure 8 with a total number of 3220 elements and 6406 nodes. Eight-node brick elements and six-node wedge elements are adopted. The mesh in the opposite boundary surfaces of the micro-RUC is exactly the same for applying the periodic boundary conditions, Equation (4), conveniently in FE analyses. The dimension of the RUC is $10 \times 200 \times 346.4$ and only one layer of element is required in the thickness direction ($x$-direction, Figure 8).

To determine the compliance matrix, six independent macroscopic deformations listed in Table 2 are considered. It is seen that either a single normal strain or a single shear strain is applied in the analysis although other combinations of deformations could also be used without altering the final results. For each case, the appropriate periodic boundary condition is determined by Equation (4) first and then applied in the FE analysis as nodal displacement constrained equations. For example, for case 5 in Table 2 the following constrained equations are applied.

For each pair of corresponding nodes on the two boundary surfaces in the $x$-direction:

$$u_x^{x+} - u_x^{x-} = 0; \quad u_y^{x+} - u_y^{x-} = 0; \quad u_z^{x+} - u_z^{x-} = 0. \tag{9a}$$

For all the corresponding nodes on the two boundary surfaces in the $y$-direction:

$$u_x^{y+} - u_x^{y-} = 0; \quad u_y^{y+} - u_y^{y-} = 0; \quad u_z^{y+} - u_z^{y-} = 0.002 \times 346.4. \tag{9b}$$

And for all the corresponding nodes on the two boundary surfaces in the $z$-direction:

$$u_x^{z+} - u_x^{z-} = 0; \quad u_y^{z+} - u_y^{z-} = 0.002 \times 200; \quad u_z^{z+} - u_z^{z-} = 0.$$

MSC NASTRAN software is used in the analysis and the boundary conditions are applied by using the multi-point constraint (MPC) technique. Detailed stress distributions can be obtained by the NASTRAN code case by case. As an example, Figure 9 shows the

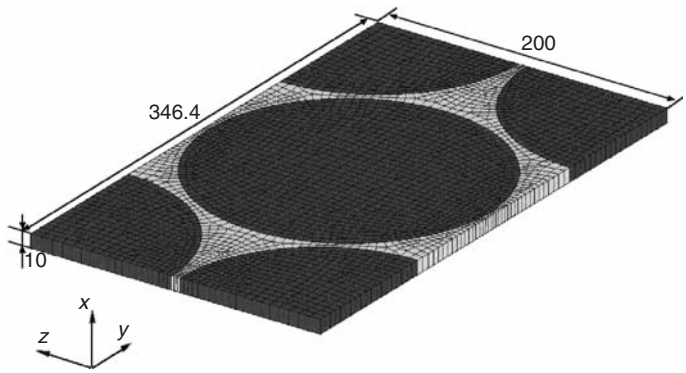


***Figure 8.*** *Finite element model of yarns.*

***Table 2. Six applied strain cases.***

| | $\varepsilon_x$ | $\varepsilon_y$ | $\varepsilon_z$ | $\gamma_{xy}$ | $\gamma_{yz}$ | $\gamma_{zx}$ |
|---|---|---|---|---|---|---|
| 1 | 0.001 | 0 | 0 | 0 | 0 | 0 |
| 2 | 0 | 0.001 | 0 | 0 | 0 | 0 |
| 3 | 0 | 0 | 0.001 | 0 | 0 | 0 |
| 4 | 0 | 0 | 0 | 0.002 | 0 | 0 |
| 5 | 0 | 0 | 0 | 0 | 0.002 | 0 |
| 6 | 0 | 0 | 0 | 0 | 0 | 0.002 |

von-Mises stress distribution together with the deformation of the micro-RUC of yarn for case 5. It can be clearly seen that the boundary faces are no longer planes and that stresses at the pair of opposite parallel boundaries are the same, i.e., the traction continuous conditions are also satisfied besides the satisfaction of deformation continuous conditions.

The corresponding global stress vector to each applied global strain vector can be computed by using Equation (5). Thus, Equation (6) can be expanded as a matrix equation,

$$[\{\bar{\varepsilon}\}_1,\ldots,\{\bar{\varepsilon}\}_6] = [S][\{\bar{\sigma}\}_1,\ldots,\{\bar{\sigma}\}_6] \tag{10}$$

and the compliance matrix $[S]$ can then be determined by:

$$[S] = [\{\bar{\varepsilon}\}_1,\ldots,\{\bar{\varepsilon}\}_6][\{\bar{\sigma}\}_1,\ldots,\{\bar{\sigma}\}_6]^{-1}. \tag{11}$$

Then all elastic constants can be acquired from the matrix $[S]$. Part of elastic constants of the yarns are listed in Table 3 and the elastic constants of yarns not listed are $\upsilon_{21}=0.091$, $\upsilon_{31}=0.091$, $\upsilon_{23}=0.296$, and $\upsilon_{32}=0.296$. For comparisons, predictions based on the other two methods [20,21] are also listed in Table 3. In both methods, $E_{11}$ and $\upsilon_{12}$ are calculated from:

$$\begin{aligned} E_{11} &= E_f V_f + E_m(1 - V_f) \\ \upsilon_{12} &= \upsilon_f V_f + \upsilon_m(1 - V_f). \end{aligned} \tag{12}$$

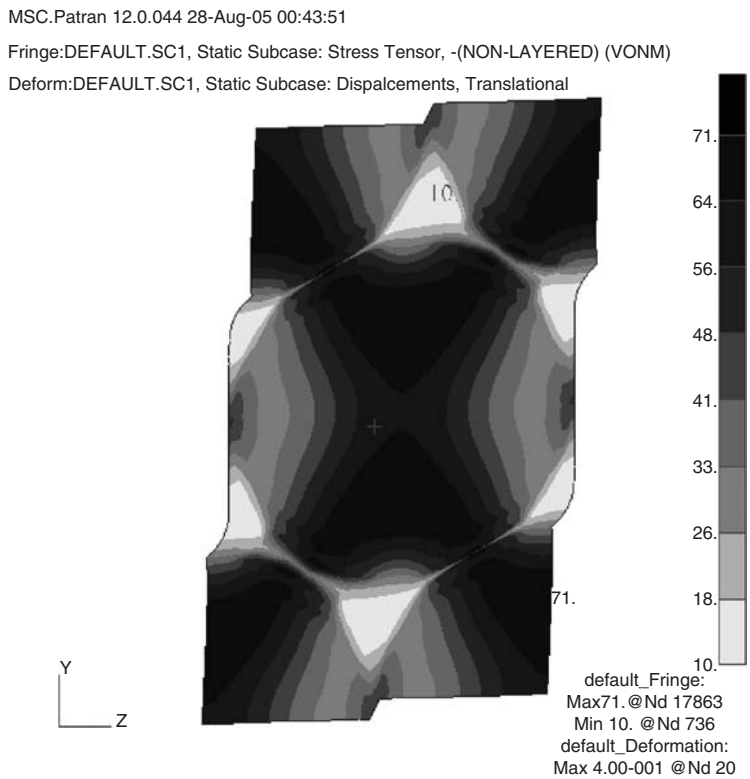


***Figure 9.*** *Deformation and von-Mises contour for case 5.*

***Table 3. Comparisons of material parameters of yarns.***

| Elastic constants | $E_{11}$ (GPa) | $E_{22}$ (GPa) | $E_{33}$ (GPa) | $G_{12}$ (GPa) | $G_{13}$ (GPa) | $G_{23}$ (GPa) | $\upsilon_{12}$ | $\upsilon_{13}$ |
|---|---|---|---|---|---|---|---|---|
| Present results | 75.86 | 34.08 | 34.13 | 12.81 | 12.85 | 13.15 | 0.204 | 0.209 |
| Analytical results | 75.28 | 32.59 | | 12.56 | | 12.92 | 0.219 | |
| Halpin–Tsai results | 75.28 | 34.27 | | 13.29 | | 14.09 | 0.219 | |

The following formulae are used [20] to get the other three constants, namely:

$$E_{22} = \frac{E_f E_m (V_f + \eta_2 (1 - V_f))}{E_m V_f + E_f \eta_2 (1 - V_f)}$$

$$G_{12} = \frac{G_f G_m (V_f + \eta_{12} (1 - V_f))}{G_m V_f + G_f \eta_{12} (1 - V_f)} \tag{13}$$

$$G_{23} = \frac{G_m}{1 - \sqrt{V_f}(1 - G_m / G_{f23})}$$

where $\eta_2$ and $\eta_{12}$ are constants to be determined by experiments. These two constants could be chosen as 0.5 for fiberglass composites [20]; however, they may depend on the fiber volume fraction.

In Reference [21], the remaining three elastic constants are calculated by the well-known Halpin–Tsai equation:

$$\frac{M}{M_m} = \frac{1 + \alpha\eta V_f}{1 - \eta V_f} \tag{14}$$

where $\eta = [(M_f/M_m) - 1]/[(M_f/M_m) + \alpha]$ and $M$ is any one of the remaining elastic constants, i.e., $E_{22}$, $G_{12}$, or $\upsilon_{23}$; $M_f$ is the corresponding elastic constants of fibers, $E_f$, $G_f$, or $\upsilon_f$; and $M_m$ is the corresponding elastic constants of matrix, $E_m$, $G_m$, or $\upsilon_m$. The value of parameter $\alpha$ varying from zero to infinity depends on geometrical and loading conditions. Typically, $\alpha = 1.3$ for computing transverse elastic constants of fiberglass composites.

From Table 3 it is found that the predicted results by current methods are in good agreement with the empirical formula (Equations (12)–(14)). The predictions also show the validity of the transversely isotropic assumption. Therefore, the correctness of the FE model as well as the periodic boundary condition is verified. Since modifications by experimental data are not required for the FE predictions, this is an advantage of the present microanalysis over the existing micro-mechanical method and Halpin–Tsai equations, which have parameters depending on constituents and geometrical structures and being determined by experiment. In addition, the present method can also yield accurate stress distributions within the yarn, thus providing the possibility for multi-scale progressive damage analysis of textile composites.

## Predicted Material Parameters for 3D Woven Composites

The complicated geometrical structure creates an obstacle on the FE mesh generation. In the present analysis, a quarter model of the RUC of 3D woven composites is meshed first due to the symmetry of the RUC, then reflected twice in the longitudinal and transverse direction to build the entire FE model, shown in Figure 10. Three types of elements, namely four-node linear tetragonal element, eight-node brick element, as well as six-node wedge element, are used in the model. To achieve the strain and stress continuous between yarns and matrix, the co-node technique is used during the meshing process. The model contains 83,141 nodes and 298,876 elements. Similar procedures to yarns described in detail previously are followed to determine the elastic constants of the 3D woven orthogonal interlock composites. During the finite element analyses, six sets of periodic

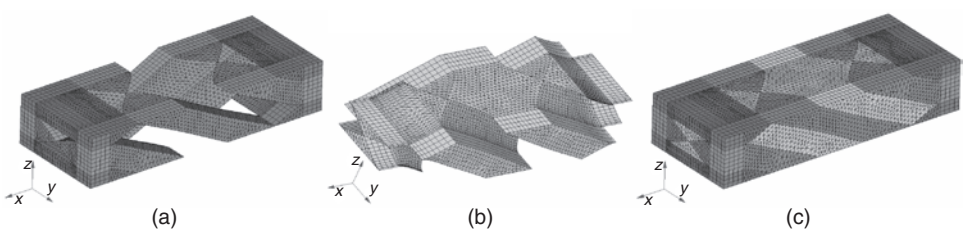


***Figure 10.*** *Finite element meshes of a quarter of the RUC: (a) mesh of yarns; (b) mesh of matrix; and (c) mesh of yarns and matrix.*

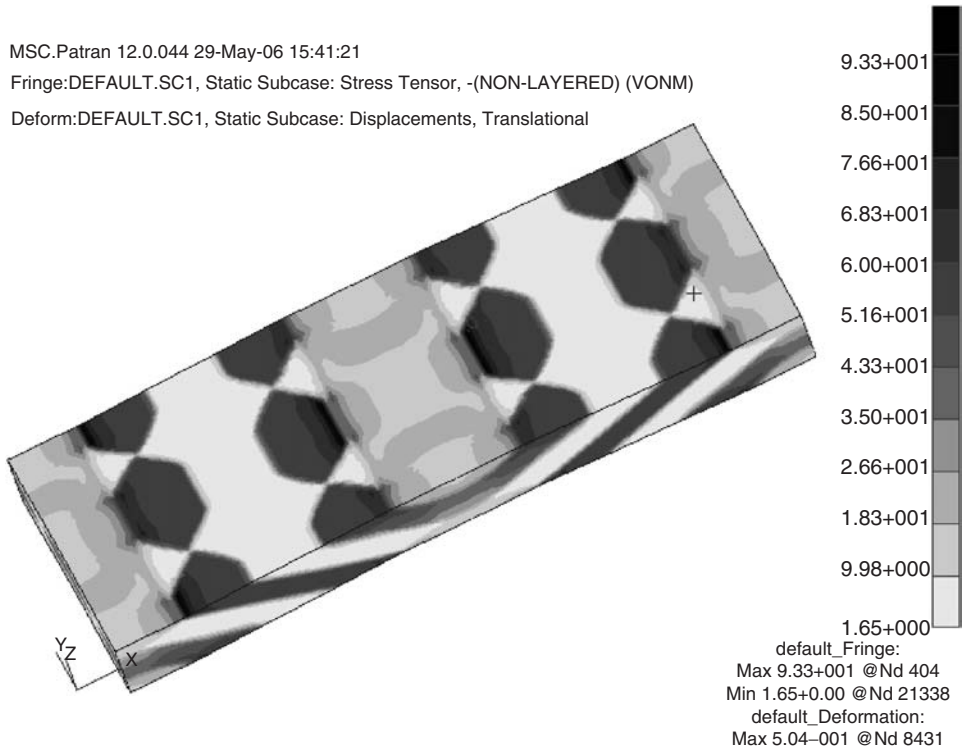


***Figure 11.*** *Deformation and von-Mises contour for case 1.*

boundary conditions are considered. The compliance matrix and elastic constants are then calculated from Equation (11).

Figure 11 shows the von-Mises stress distributions plotted on the deformed meso-RUC for case 1. The continuity conditions of deformation and tractions are satisfied strictly in the present analysis. It is noted that the two boundary surfaces in the $z$-direction are no longer planes after deformation, even though only the uniform global normal strain is applied. The 3D FE technique can yield detailed accurate stress distributions. It is seen that the warp yarns carry most of the applied load and stress concentration appears in the intersection regions between the warp yarns and weft yarns.

Figure 12 shows the von-Mises stress distributions plotted on the deformed meso-RUC for case 4. It should be pointed out again that the continuity conditions of deformation and tractions are satisfied strictly and the boundary surfaces do not remain planes after deformation for pure shear strain loadings, a phenomenon observed previously. The stress concentration is more visible for the shear loadings. The maximum stress is in intersection regions of neighboring warp yarns. The stress concentration is also presented in regions between warp yarns and weft yarns and between the yarns and matrix.

The predicted elastic constants of 3D woven composites are listed in Table 4. To verify the predicted results, a 3D woven composite was fabricated and test specimens were then manufactured with a house-made resin transfer molding (RTM) equipment. Strain gauges were mounted on the specimen along the longitudinal and transverse directions. Tensile experiments were performed on the WDW-E2000 test machine and the longitudinal and

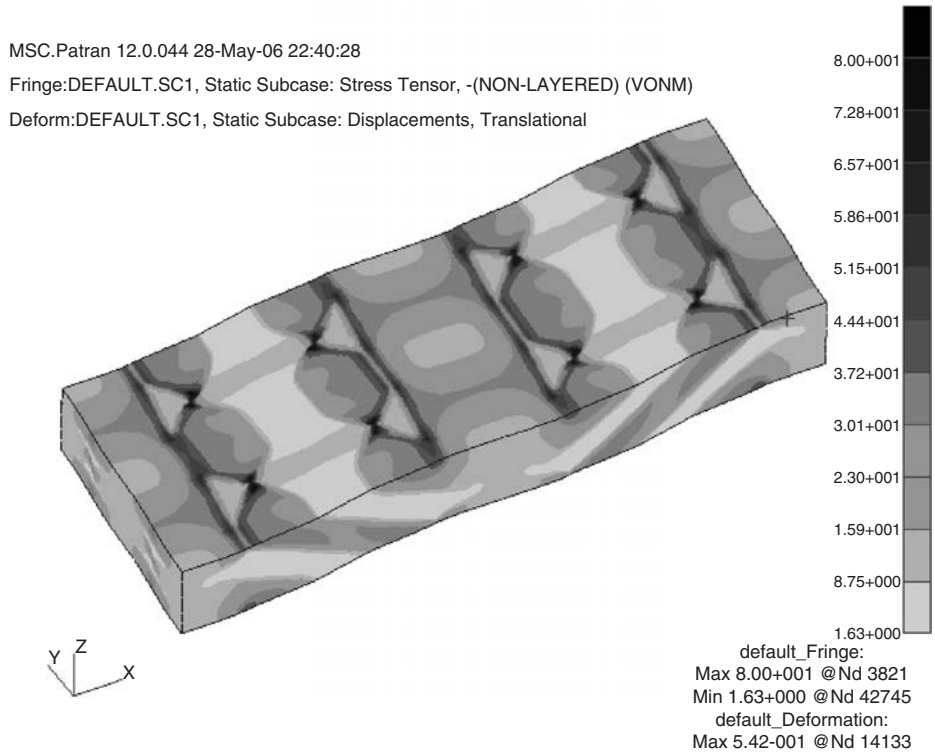


***Figure 12.*** *Deformation and von-Mises contour for case 4.*

***Table 4. Parameters of 3D woven composite (unit: GPa).***

| **Parameter** | $E_1$ | $E_2$ | $E_3$ | $G_{23}$ |
|---|---|---|---|---|
| FEM result | 16.34 | 11.53 | 10.41 | 2.50 |
| Parameter | $G_{31}$ | $G_{12}$ | $\nu_{12}$ | $\nu_{13}$ |
| FEM result | 2.07 | 2.53 | 0.124 | 0.319 |
| Parameter | $\nu_{23}$ | $\nu_{21}$ | $\nu_{31}$ | $\nu_{32}$ |
| FEM result | 0.346 | 0.162 | 0.512 | 0.415 |

transverse strains were recorded by strain gauges. Figure 13 shows the experimental setup. Experiment results are listed in Table 5.

From Tables 4 and 5, it can be seen that the predicted longitudinal and transverse moduli agree with the test data, although the predicted transverse modulus is a little lower than the test value, while the predicted longitudinal module is a little higher than the test result. The largest discrepancy between the prediction and test datum is in Poisson's ratio, the relative error is approximately 15%. The discrepancy between predictions and experimental data might be attributed to the fact that the FE model neglects the effect of surface yarns, which have lower volume fraction of warps and higher volume fraction of wefts.

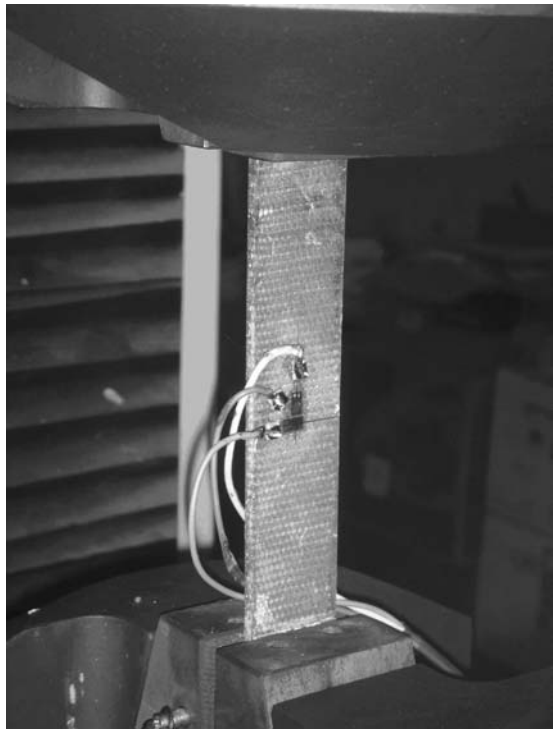

***Figure 13.*** *Photo of experimental setup.*

***Table 5. Experimental data (unit: GPa).***

| $E_1$ | $E_2$ | $\upsilon_{12}$ | $\upsilon_{21}$ |
|---|---|---|---|
| 16.14 | 12.85 | 0.108 | 0.147 |

## CONCLUSIONS

Two-scale 3D finite element (FE) models, the micro-RUC, for the yarn and the meso-RUC, are presented and used for predicting elastic moduli of 3D woven orthogonal interlock composites by FE analysis. The novel geometrical model of 3D woven orthogonal interlock composites is built based on the Hermit-spline function. The new periodic boundary conditions ensuring deformation and stress continuity on the boundary surfaces of RUCs of yarn and woven composite are used for the first time for analysis of 3D woven composites. The predicted results of yarns are in good agreement with data computed by available equations with suitable parameters determined by experimental data. The predicted properties of 3D woven composite are also in good agreement with test data. It is an obvious advantage of the present method that the properties of composites can be determined based purely on the properties of constituents and volume

fraction of each constituent without introducing modification parameters, which need to be calibrated from experiments. Since the present method can yield detailed stress distributions in two scales, it thus provides the possibility for multi-scale progressive damage analysis of textile composites. This work is currently being undertaken in our research group.

## ACKNOWLEDGMENTS

The work was partially supported by the Chinese Natural Science Foundation (10472045) and by the Nan-hang-da Bo-shi Chuang-xin Ji-jin (BCXJ04-03). Authors would like to express their special appreciation to Professor Z. Xia of the University of Alberta for his helpful suggestions in improving the manuscript.

## REFERENCES

1. Tan, P., Tong, L. and Steven, J. (1998). Modeling Approaches for 3D Orthogonal Woven Composite, *Journal of Reinforced Plastics & Composites*, **17**(6): 545–577.
2. Ding, X. and Yi, H. (2005). Representation of 3D Woven Structures by Parametric Method, *Journal of Donghua University*, **22**(1): 22–25.
3. Yan, Y. and Cheng, C. (1999). Analysis of Elastic Property for 3D Woven Composites Based on Fabric Microstructure, *Acta Aeronautica et Astronautica Sinica*, **20**(4): 289–293.
4. Lomov, S.L., Gusakov, A.V. and Huysmans, G. (2000). Textile Geometry Preprocessor for Meso-mechanical Models of Woven Composites, *Composites Science and Technology*, **60**(11): 2083–2095.
5. Ding, X. and Yi, H. (2003). A Geometric Model of Three Dimensional Woven Structures, *Acta Materiae Compositae Sinica*, **20**(5): 108–113 (in Chinese).
6. Zhou, G., Zhou, C. and Wang, X. (2004). Micromechanical Analysis of 3D Woven Composites, *Transactions of Nanjing University of Aeronautics and Astronautics*, **121**(3): 163–167 (in Chinese).
7. Yang, L. (2005). CAD on Elastic Properties of 3D Woven Composites, *Journal of Tianjin Polytechnic University*, **24**(2): 31–35 (in Chinese).
8. Whitney, T.J. and Chou, T.W. (1989). Modeling of 3D Angle-interlock Textile Structural Composites, *Journal of Composite Materials*, **23**(9): 890–911.
9. Ignaas, V. and Lomov, S.V. (2005). Virtual Textile Composites Software WiseTex: Integration with Micro-mechanical Permeability and Structural Analysis, *Composites Science and Technology*, **65**(16): 2563–2574.
10. Yi, H. and Ding, X. (2003). A Model to Predict Elastic Properties of 3D Woven Composites, *Acta Mechanica Sinica*, **35**(5): 569–577.
11. Cox, B.N., Carter, W.C. and Fleck, N.A. (1994). A Binary Model of Textile Composites: I. Formulation, *Acta Metallurgica et Materialia*, **42**(10): 3463–3479.
12. Potiuri, P., Sharma, S. and Ramgulam, R. (2001). Comprehensive Drape Modeling for Moulding 3D Textile Performs, *Composites*: *Part A*, **60**(10): 1415–1424.
13. Zeng, T. et al. (2004). Predicting the Nonlinear Response and Failure of 3D Braided Composites, *Materials Letters*, **58**(26): 3237–3241.
14. Swan, C.C. and Kim, H. (2002). Multi-scale Cell Analyses of Textile Composites, *15th ASCE Engineering Mechanics Conference*, Columbia University, New York.
15. Xia, Z. et al. (2006). On Selection of Repeated Unit Cell Model and Application of Unified Periodic Boundary Conditions in Micro-mechanical Analysis of Composites, *International Journal of Solids and Structures*, **43**(2): 266–278.

16. Xia, Z., Zhang, Y. and Ellyin, F. (2003). A Unified Periodical Boundary Conditions for Representative Volume Elements of Composites and Applications, *International Journal of Solids and Structures*, **40**(8): 1907–1921.
17. Rami, M.H. and Anastasia, H. (2004). A Multi-scale Constitutive Formulation for the Nonlinear Viscoelastic Analysis of Laminated Composite Materials and Structures, *International Journal of Solids and Structures*, **41**(13): 3461–3490.
18. Ivanov, I. and Tabiei, A. (2001). Three-dimensional Computational Micro-mechanical Model for Woven Fabric Composites, *Composite structures*, **54**(4): 489–496.
19. Carvelli, V. and Poggi, C. (2001). Numerical Prediction of the Mechanical Properties of Woven Fabric Composites, *ICCM-13*, Beijing, China.
20. Chen, S. (1990). Mechanical of Composite Materials, *Design Manual of Composite Materials*, pp. 50–62, The Aeronautical Industry Publishing, Beijing.
21. Harris, B. (1986). Elastic Properties of Fiber Composites, *Engineering Composite Materials*, Institute of Metals, London.